Composite Structures 136 (2016) 450–459

Contents lists available at ScienceDirect

Composite Structures

journal homepage: www.elsevier.com/locate/compstruct

Theoretical and experimental study on notched steel beams strengthened with CFRP plate

Jun Deng *, Yonghui Jia, Hengzhong Zheng

School of Civil and Transportation Engineering, Guangdong University of Technology, Guangzhou 510006, China

ARTICLE INFO

Article history:
Available online 26 October 2015

Keywords:
Stress analysis
CFRP
Adhesive bonding
Steel beams
Notch
Debonding

ABSTRACT

CFRP external bonding is an alternative technique to repair or strengthen notch damaged steel beams. However, the premature debonding failure caused by the stress concentration at the notch location reduces the effectiveness of this reinforcement technique. This paper presents an integrated closed-form solution for obtaining the interfacial shear and normal stresses in steel beams strengthened with a CFRP plate. Simple expressions of the maximum interfacial stresses at the notch locations, the adhesive hollows and the plate ends are given. A parametric study indicates that the maximum stresses at the notch locations increased with the notch depth and the applied bending moment on notched cross-sections, but reduced with the thickness of the adhesive. An experimental study of model-scale CFRP bonded steel beams was conducted as well. The test results show the strength of the notched beam can be improved almost twice by the CFRP plate strengthening, while the brittle fracture caused by intermediate debonding initiated from the notch location limits the ductility enhancement of the retrofitted beams. The good agreement between the longitudinal strain distributions in the CFRP plate obtained from the tests and the corresponding analytical results demonstrates the validity of the theory.

1. Introduction

The application of FRP in upgrading and retrofitting concrete structures are worldwide as reinforcing using FRP is cheaper and better than conventional materials and techniques. Since the use of FRP provides a cost saving in the region of around 18% over steel, FRP strengthening is becoming an attractive technique for extending the life of metallic structures as well [1]. Over 25% of bridges in the United States, of which almost 50% are made of steel, are structural deficient or functionally obsolete [2]. The fatigue-induced cracks in steel beams are critical to their service life, which demonstrates the need for repairing. However, the performance of CFRP used for cracked steel beams is known very little [3].

Previous research has been established CFRP external bonding as a promising alternative strengthening technique for steel [4–5]. Rizkalla et al. [6] and Colombi and Poggi [7] has shown that the load-carrying capacity of steel beams are significantly improve by applying CFRP materials. Sen et al. [8] and Deng et al. [9] report the improvement in stiffness of steel beams when bonded with CFRP plates. To simulate the structural damage in laboratory, part of the tension flange of steel beams is saw-cut [10]. The experimental results showed that the CFRP repaired cracked beams achieved various levels of recovery, and in some cases, exceeded the original capacities. Hmidan et al. [11] reports that the level of initial damage affects the behaviour of a plastic region above the notch tip, the rate of web fracture and the initiation of CFRP debonding, but the failure mode.

Buyukozturk et al. [12], Smith and Teng [13] and Deng and Lee [14] have confirmed that the adhesive bonding is the weakest link in steel strengthening owing to the high stress concentration. Analytical and numerical solution [15] and FE analysis [16,17] were conducted to calculate the stress concentration at the plate ends of the CFRP strengthened steel beams. Several FE modelling approaches [3,18,19] were developed to investigate the stress concentration resulting at the notch locations in the steel beam. The stress concentrations also conduct fatigue interfacial failure at the plate ends [20] or at the crack locations [21]. Colombi and Fava [21] indicated that reinforcement debonding has a detrimental effect on the reinforcement effectiveness and it lessens the fatigue life.

Teng et al. [17] indicated that very limits research is available on intermediate debonding in CFRP-strengthened steel beams and no theoretical modelling exists so far. Colombi and Fava [21] summarised an analytical approach to calculate the maximum shear stress in the adhesive layer at the crack location. However, the shear force applied on the retrofitted beams was not considered in the analytical solution. Interfacial normal stresses,

* Corresponding author.

http://dx.doi.org/10.1016/j.compstruct.2015.10.024
0263-8223/

which has significant effect on the stress concentration at the plate ends as shown in literature [15], were not been considered as well.

As a further development of the solutions by Deng et al. [15], this paper presents an integrated closed-form solution for obtaining the interfacial shear and normal stresses in a retrofitted steel beam (Fig. 1). The simple expressions of the maximum interfacial stresses at the notch locations, the adhesive hollows and the plate ends are developed. A parametric study is conducted to compare the results of models with different notch location, notch depth and adhesive thickness. An experimental study of model-scale CFRP bonded steel beams is reported as well. The effect of CFRP strengthening on the load-capability, stiffness and failure modes of the notched beams are evaluated. The test results also used to validate the analytical solutions.

2. Interfacial stress analysis

The theoretical expressions of the longitudinal tension of the CFRP plate and the interfacial stresses of the retrofitted steel beams are presented in this section. The analytical solutions of the maximum interfacial stresses at the notch locations, the adhesive hollows and the plate ends are given as well.

2.1. Longitudinal tension of CFRP plate

Fig. 2 shows an infinitesimal element of a steel beam strengthened with a CFRP plate, of length dx and width b. The longitudinal tension and shear force at the ends of the adhesive are ignored. In the figure, M, V and N are the bending moment, the shear force and the longitudinal tension, respectively, τ and σ the shear stress and the normal stress at the interface, respectively, Z_s, Z_f and t_a the distance from the neutral axis to the bottom of the steel beam, the

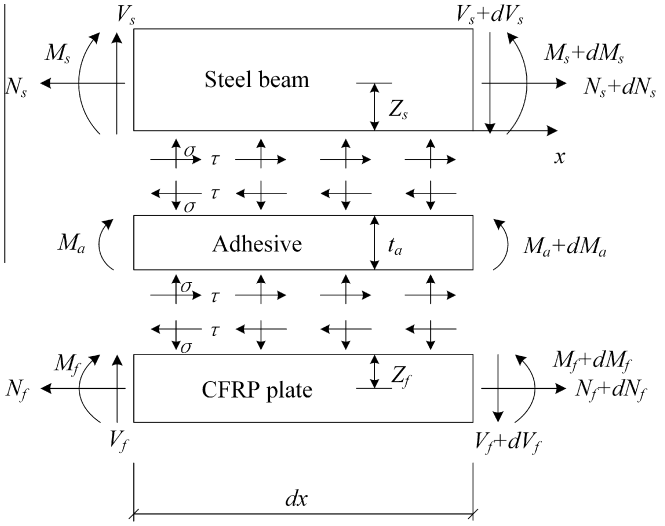

Fig. 2. An infinitesimal element of a retrofitted beam.

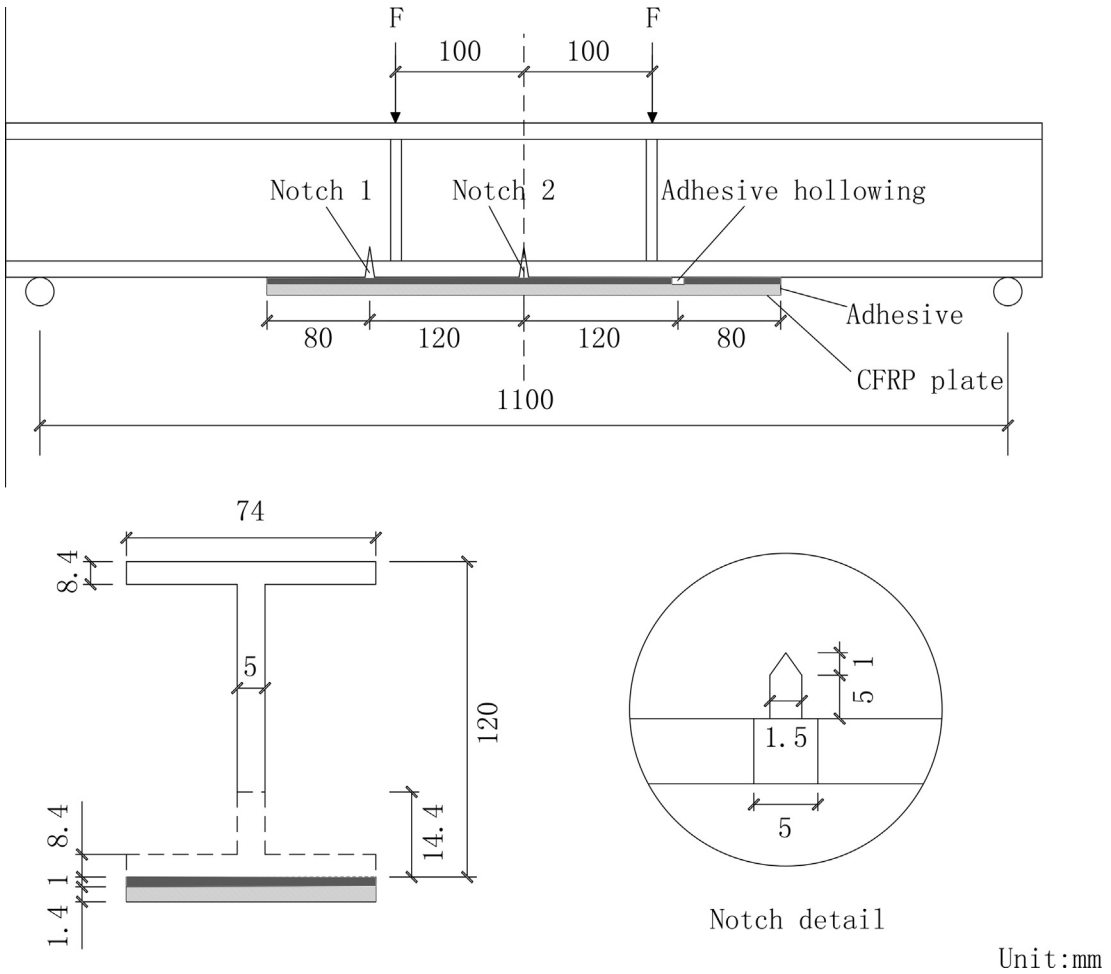

Fig. 1. Details of the retrofitted beam.

distance from the neutral axis to the top of the CFRP plate and the adhesive thickness. The subscripts *s*, *f* and *a* denote steel beam, CFRP plate and adhesive, respectively. This notation will be used throughout the paper.

All materials considered are linear elastic. For the steel beam, the longitudinal force, transverse force and moment equilibria of the element can be expressed, respectively, as:

$$\frac{1}{b}\frac{dN_s}{dx} = -\tau \tag{1}$$

$$\frac{dV_s}{dx} = b\sigma \tag{2}$$

$$\frac{dM_s}{dx} = V_s - \tau b Z_s \tag{3}$$

Neglecting bending of the CFRP plate and assuming the shear stress in the adhesive layer do not vary through the thickness of the adhesive, the shear stress–strain relationship of the adhesive can be given as:

$$\frac{d\tau}{dx} = -\frac{G}{t_a}(\varepsilon_s - \varepsilon_f) \tag{4}$$

where ε_s and ε_f are the strain at the bottom of the steel beam and the top of the CFRP plate, respectively, and they are given as:

$$\varepsilon_s = \alpha_s \Delta T - \frac{M_p Z_s}{E_s I_s} + \frac{M_s Z_s}{E_s I_s} + \frac{N_s}{E_s A_s} \tag{5}$$

$$\varepsilon_f = \alpha_f \Delta T - \frac{F_p}{E_f I_f} - \frac{M_f Z_f}{E_f I_f} + \frac{N_f}{E_f A_f} \tag{6}$$

where α and ΔT are the thermal expansion coefficient and the temperature change, respectively, E, I and A the elastic modulus, the second moment of area and the area, respectively, M_p the bending moment applied on the steel beam by load-relief jacking, F_p the prestressing force applied on the CFRP.

For the combined cross section, the force equilibrium in the longitudinal direction and the moment equilibrium can be described, respectively, as:

$$N_s = -N_f \tag{7}$$

$$M_s + M_f + N_f(Z_s + Z_f) = M_1 \tag{8}$$

where M_1 is the applied moment. Ignoring M_f, Eq. (8) gives:

$$M_s = -N_f(Z_s + Z_f) + M_1 \tag{9}$$

Differentiating Eq. (1) with respect to x and substituting Eqs. (4), (7) and (9) gives the governing equation of N_f:

$$\frac{d^2 N_f}{dx^2} - \lambda^2 N_f + \lambda^2 \frac{\Delta\varepsilon_{sf}}{f_2} = 0 \tag{10}$$

where

$$\lambda = \sqrt{\frac{f_2}{f_1}} \tag{11}$$

$$f_1 = \frac{t_a}{Gb} \tag{12}$$

$$f_2 = \frac{(Z_s + Z_f)Z_s}{E_s I_s} + \frac{1}{E_s A_s} + \frac{1}{E_f A_f} \tag{13}$$

$$\Delta\varepsilon_{sf} = (\alpha_s - \alpha_f)\Delta T - \frac{M_p Z_s}{E_s I_s} + \frac{F_p}{E_f A_f} + \frac{M_1 Z_s}{E_s I_s} \tag{14}$$

$\Delta\varepsilon_{sf}$ is the relative deformation between the bottom of the steel beam and the top of CFRP plate when the adhesive layer is ignored, including the relative deformations caused by temperature change, load-relief jacking, prestressing force and applied moment.

The solution of Eq. (10) has the general solution in the form:

$$N_f = c_1 e^{-\lambda x} + c_2 e^{\lambda x} + \frac{\Delta\varepsilon_{sf}}{f_2} \tag{15}$$

The boundary conditions include N_f at the ends of the CFRP, the notch locations and the hollowing in the adhesive layer. Submitting N_{f1} and N_{f2} which are N_f at the boundaries located at $x = l_1$ and $x = l_2$ gives:

$$c_1 = \frac{\left(N_{f1} - \frac{\Delta\varepsilon_{sf1}}{f_2}\right)e^{\lambda l_2} - \left(N_{f2} - \frac{\Delta\varepsilon_{sf2}}{f_2}\right)e^{\lambda l_1}}{e^{\lambda(-l_1+l_2)} - e^{\lambda(l_1-l_2)}} \tag{16}$$

$$c_2 = \frac{\left(N_{f1} - \frac{\Delta\varepsilon_{sf1}}{f_2}\right)e^{-\lambda l_2} - \left(N_{f2} - \frac{\Delta\varepsilon_{sf2}}{f_2}\right)e^{-\lambda l_1}}{e^{\lambda(l_1-l_2)} - e^{\lambda(-l_1+l_2)}} \tag{17}$$

When the boundaries are close, $l_2 - l_1 > 0$, Eqs. (16) and (17) can be simplified as:

$$c_1 = \left(N_{f1} - \frac{\Delta\varepsilon_{sf1}}{f_2}\right)e^{\lambda l_1} - \left(N_{f2} - \frac{\Delta\varepsilon_{sf2}}{f_2}\right)e^{\lambda(2l_1-l_2)} \tag{18}$$

$$c_2 = -\left(N_{f1} - \frac{\Delta\varepsilon_{sf1}}{f_2}\right)e^{\lambda(l_1-2l_2)} + \left(N_{f2} - \frac{\Delta\varepsilon_{sf2}}{f_2}\right)e^{-\lambda l_2} \tag{19}$$

When the boundaries are distant, $l_2 - l_1 >> 0$, Eqs. (16) and (17) can be simplified as:

$$c_1 = \left(N_{f1} - \frac{\Delta\varepsilon_{sf1}}{f_2}\right)e^{\lambda l_1} \tag{20}$$

$$c_2 = \left(N_{f2} - \frac{\Delta\varepsilon_{sf2}}{f_2}\right)e^{-\lambda l_2} \tag{21}$$

When the origin of X-axis locates at the first boundary, $l_1 = 0$, c_2 can be ignored and Eq. (20) can be simplified as:

$$c = N_{f0} - \frac{\Delta\varepsilon_{sf}}{f_2} \tag{22}$$

where c replaces c_1 and N_{f0} is the longitudinal tension at the first boundary.

The longitudinal tension at different boundaries, N_{f1}, N_{f2} or N_{f0}, can be obtained as following:

(1) At the end of the CFRP plate: $N_f = 0$.

(2) At the notch locations, the moment equilibrium of the combined cross section can be described as:

$$N_f(Z'_s + a + t_a + Z_f) + M_s = M_1 \tag{23}$$

where a is the notch depth. Assuming plane sections remaining plane, the deformation compatibility of the cross section at the notch locations can be expressed as:

$$\frac{M_s(Z'_s + a + t_a + Z_f)}{E_s I'_s} - \frac{N_f}{E_s A'_s} = \frac{N_f}{E_f A_f} \tag{24}$$

where A'_s, I'_s and Z'_s are the area, the second moment of area and the distance from the neutral axis to the notch tip at the notch sections, respectively. Substituting Eq. (23) into Eq. (24) gives:

$$N_f = \frac{\Delta\varepsilon'_{sf}}{f'_2} \tag{25}$$

where

$$\Delta\varepsilon'_{sf} = \frac{M_1(Z'_s + a + t_a + Z_f)}{E_s I'_s} \tag{26}$$

$$f_2' = \frac{(Z_s' + a + t_a + Z_f)^2}{E_s I_s'} + \frac{1}{E_s A_s'} + \frac{1}{E_f A_f} \tag{27}$$

(3) At the locations of the hollowing in the adhesive layer, N_f can be obtained from Eq. (25) as well, in which $a = 0$, $Z_s' = Z_s$, $A_s' = A_s$, $I_s' = I_s$.

2.2. Shear stress

Substituting Eq. (7) into Eq. (1) gives:

$$\tau = \frac{1}{b}\frac{dN_f}{dx} = -\frac{1}{b}\lambda c_1 e^{-\lambda x} + \frac{1}{b}\lambda c_2 e^{\lambda x} + \frac{1}{bf_2}\frac{d\Delta e_{sf}}{dx} \tag{28}$$

Substituting Eq. (14) into the above equation gives:

$$\tau = -\frac{1}{b}\lambda c_1 e^{-\lambda x} + \frac{1}{b}\lambda c_2 e^{\lambda x} + \frac{Z_s}{bf_2 E_s I_s}(V_1(x) - V_p(x)) \tag{29}$$

where $V_1(x)$ and $V_p(x)$ are the shear forces caused by applied loading and load-relief jacking.

When the origin of X-axis locates at the boundary, Eq. (29) can be simplified as:

$$\tau = -\frac{\lambda c}{b}e^{-\lambda x} + \frac{Z_s}{bf_2 E_s I_s}(V_1(x) - V_p(x)) \tag{30}$$

2.3. Normal stress

Assuming the normal stress in the adhesive layer do not vary through the thickness, the normal stress can be described as:

$$\sigma = \frac{E_a}{t_a}(v_f - v_s) \tag{31}$$

v_s and v_f are the transverse displacements at the bottom of the beam and the top of the plate, respectively, which are given as:

$$\frac{d^2 v_s(x)}{dx^2} = \frac{M_s(x)}{E_s I_s} \tag{32}$$

$$\frac{d^2 v_f(x)}{dx^2} = \frac{M_f(x)}{E_f I_f} \tag{33}$$

Differentiating Eq. (31) four times with respect to x and Substituting Eqs. (1)–(3), (8), (32) and (33) give the governing equation:

$$f_3\frac{d^4\sigma}{dx^4} + f_4\sigma - f_5\frac{d\tau}{dx} - \frac{q}{bE_s I_s} = 0 \tag{34}$$

where q is distributed load applied on the beam,

$$f_3 = \frac{t_a}{E_a b} \tag{35}$$

$$f_4 = \frac{1}{E_f I_f} + \frac{1}{E_s I_s} \tag{36}$$

$$f_5 = \frac{Z_s}{E_s I_s} - \frac{Z_f}{E_f I_f} \tag{37}$$

Ignoring the small term including q, the general solution to Eq. (34) is:

$$\sigma(x) = e^{-\beta x}(s_1\cos(\beta x) + s_2\sin(\beta x)) + \frac{f_5}{f_4}\frac{d\tau}{dx} \tag{38}$$

where

$$\beta = \sqrt[4]{\frac{f_4}{4f_3}} \tag{39}$$

The boundary conditions are employed to obtained s_1 and s_2.

(1) At the ends of the CFRP plate, the bending moment and shear force of the CFRP plate are zero. Differentiating Eq. (31) two times and three times give the boundary conditions, respectively:

$$\frac{d^2\sigma(0)}{dx^2} = \frac{E_a}{t_a}\left(\frac{M_f}{E_f I_f} - \frac{M_s}{E_s I_s}\right) = -\frac{E_a}{t_a}\frac{M_1(0)}{E_s I_s} \tag{40}$$

$$\frac{d^3\sigma(0)}{dx^3} = \frac{f_5}{f_3}\tau(0) - \frac{E_a}{t_a}\frac{V_1(0)}{E_s I_s} \tag{41}$$

Combining (30), (38), (40) and (41) gives, respectively,

$$s_1 = \frac{c}{2\beta^3 b}\left(-\frac{f_5}{f_3}\lambda + \frac{f_5}{f_4}\lambda^5 - \beta\frac{f_5}{f_4}\lambda^4\right) + \frac{1}{2\beta^3}\left(\frac{f_5 Z_s}{f_3 bf_2 E_s I_s}V_1(0) - \frac{\beta E_a}{t_a}\frac{M_1(0)}{E_s I_s} - \frac{E_a}{t_a}\frac{V_1(0)}{E_s I_s}\right) \tag{42}$$

$$s_2 = \frac{1}{2\beta^2}\left(\frac{E_a}{t_a}\frac{M_1(0)}{E_s I_s} + \frac{f_5}{f_4}\frac{c}{b}\lambda^4\right) \tag{43}$$

(2) At the notch locations, $V_f = 0$. Assuming the flexure of the CFRP plate is continued at the notched cross sections gives:

$$\frac{M_f}{E_f I_f} = \frac{M_1}{\overline{EI}} \tag{44}$$

where $\overline{EI}$ is the combined stiffness of the strengthened sections,

$$\overline{EI} = E_s I_s + E_f I_f + (Z_s + Z_f)^2\overline{EA} \tag{45}$$

$$\frac{1}{\overline{EA}} = \frac{1}{E_s A_s} + \frac{1}{E_f A_f} \tag{46}$$

Assuming plane sections remaining plane at the notched cross-sections gives:

$$\frac{M_s}{E_s I_s} = \frac{M_1}{(\overline{EI})'} \tag{47}$$

where $(\overline{EI})'$ is the combined stiffness of the strengthened notched sections,

$$(\overline{EI})' = E_s I_s' + E_f I_f + (Z_s' + a + Z_f)^2(\overline{EA})' \tag{48}$$

$$\frac{1}{(\overline{EA})'} = \frac{1}{E_s A_s'} + \frac{1}{E_f A_f} \tag{49}$$

If

$$\frac{1}{(\overline{EI})_1} = \frac{1}{(\overline{EI})'} - \frac{1}{\overline{EI}} \tag{50}$$

Eq. (40) can be expressed as:

$$\frac{d^2\sigma(0)}{dx^2} = \frac{E_a}{t_a}\left(\frac{M_f}{E_f I_f} - \frac{M_s}{E_s I_s}\right) = -\frac{E_a}{t_a}\frac{M_1(0)}{(\overline{EI})_1} \tag{51}$$

Combining Eqs. (41) and (51) gives:

$$s_1 = \frac{c}{2\beta^3 b}\left(-\frac{f_5}{f_3}\lambda + \frac{f_5}{f_4}\lambda^5 - \beta\frac{f_5}{f_4}\lambda^4\right) + \frac{1}{2\beta^3}\left(\frac{f_5 Z_s}{f_3 bf_2 E_s I_s}V_1(0) - \frac{\beta E_a}{t_a}\frac{M_1(0)}{(\overline{EI})_1} - \frac{E_a}{t_a}\frac{V_1(0)}{E_s I_s}\right) \tag{52}$$

$$s_2 = \frac{1}{2\beta^2}\left(\frac{E_a}{t_a}\frac{M_1(0)}{(\overline{EI})_1} + \frac{f_5}{f_4}\frac{c}{b}\lambda^4\right) \tag{53}$$

(3) At the locations of the hollowing in the adhesive layer,

$$\frac{d^2\sigma(0)}{dx^2} = \frac{E_a}{t_a}\left(\frac{M_f}{E_f I_f} - \frac{M_s}{E_s I_s}\right) = 0 \tag{54}$$

Combining Eqs. (41) and (54) gives s_1 and s_2.

2.4. Maximum stresses

On the right side of the boundaries, the maximum shear stress τ_{max} can be written as:

$$\tau_{\max} = -\frac{1}{b}\lambda c + \frac{Z_s}{bf_2 E_s I_s} V(0) \tag{55}$$

On the left side of the boundaries, the direction of τ_{max} is opposite. At the boundaries, normal stress σ_{max} can be written as:

$$\sigma_{\max} = (\beta - \frac{\lambda}{2})\frac{t_f \lambda}{b} c - \frac{\beta t_f Z_s}{bf_2 E_s I_s} V(0) \tag{56}$$

Combining the maximum shear and normal stresses, the maximum tensile principal stress σ_{1max} can be written as:

$$\sigma_{1\max} = -\frac{\sigma_{\max}}{2} + \sqrt{\left(\frac{\sigma_{\max}}{2}\right)^2 + \tau_{\max}^2} \tag{57}$$

3. Analytical results and parametric analysis

An example was employed to compare the analytical interfacial stresses at different boundaries, including the notches, the adhesive hollowing and the plate ends. To investigate the effects of the notch location and notch depth on the maximum interfacial stresses, furthermore, a parametric analysis was performed.

3.1. Analytical results

The geometry of the retrofitted beam is shown in Fig. 1. The clear span of the beam was 1.1 m and the loading points were 200 mm apart. The steel beams used were 1.2 m long I beam with a height of 120 mm, a flange width of 74 mm, a flange thickness of 8.4 mm and a web thickness of 5 mm. The steel had an yield strength of 305.3 MPa and a Young's modulus of 205.1 GPa. The CFRP plate had a length of 400 mm, a width of 74 mm and a thickness of 1.4 mm, a Young's modulus of 127.2 GPa and a tensile strength of 745.9 MPa. The thick of adhesive layer was 1 mm. The adhesive had a Young's modulus of 11.2 GPa, a shear modulus of 4.3 GPa and a tensile strength of 25.5 MPa. In order to observe the effect of different boundaries on the interfacial stresses, two notches in the steel beam and one hollowing in the adhesive layer are considered. The notch depth was 14.4 mm as shown in Fig. 1.

The longitudinal tensile distribution in the CFRP plate calculated by Eq. (15) is shown in Fig. 3 when the concentrated loads P are equal to 35 kN. As shown in the figure, the longitudinal tensions rapidly increase near the ends of the plate and the notches. The most obvious longitudinal tensions occur at the notches where the tensile stresses in the section of the retrofitted beam mainly provided by the CFRP plate. The interfacial shear and normal stresses calculated by Eqs. (29) and (38) are shown in Fig. 4. As shown in the figure, high stress concentrations occur at the ends of adhesively bonded plates and the notch locations, while the stress concentration at the location of the hollowing is marginal. The results of the stress concentrations calculated by Eqs. (55)–(57) are shown in Table 1. As shown in the table, the maximum tensile principle stress at the notch in the middle of the beam is about two times than that at the ends of the plate, which indicates that the stress concentration at notch location is the major weakness of this bonded beam.

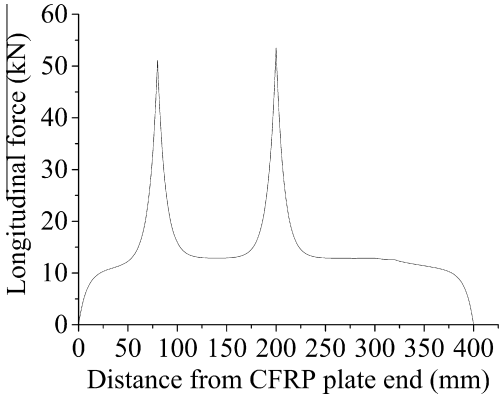

Fig. 3. Distribution of longitudinal force in CFRP plate.

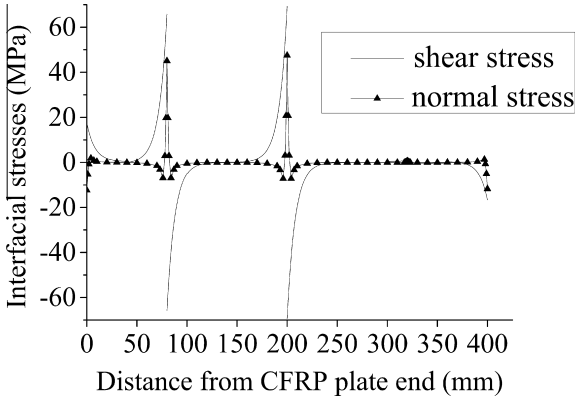

Fig. 4. Distribution of interfacial stresses.

Table 1
Results of the shear and normal stress concentrations in different locations.

Location	Maximum shear stress (MPa)	Maximum normal stress (MPa)	Maximum tensile principle stress (MPa)
Notch 1	65.8	45.5	46.9
Notch 2	69.3	47.9	49.4
CFRP plate ends	−17.4	−12.1	24.5
Adhesive hollowing	0.9	0.7	0.7

3.2. Parametric study

The maximum values of the shear and normal interfacial stresses in retrofitted beams are influenced by various parameters of which the thickness of the adhesive layer is the most significant one and is regularly increased to reduce the stress concentration in engineering applications [15]. For retrofitted notched beams, the most important ones are the depth and the location of the notches. These parameters were studied using the analytical solutions.

Figs. 5–7 plot the maximum stresses versus the various notch and adhesive parameters. Fig. 5 shows that the maximum stresses increase rapidly when the notch only in the flange and then linearly after the notch develops into the web. It is because the second moment of area of the notched cross-section varies significantly with the notch depth in the flange. Fig. 6 shows that the maximum stresses increase linearly with the distance of the notches apart from the supporter up to the pure bending moment zone between the two loading points. It indicates that the applied bending moment of the notched cross-sections has near linear

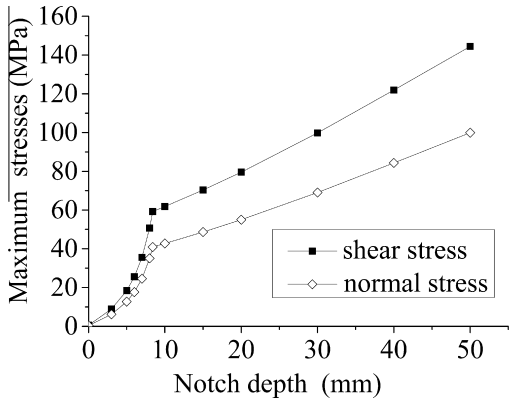

Fig. 5. Maximum interfacial stresses with different notch depth.

relationship with the maximum stresses. Fig. 7 shows that the maximum stresses reduced with the thickness of the adhesive, which is in agreement with the results at the plate ends [15].

4. Experimental study

In order to validate the theoretical results of stress analysis, the longitudinal tension on the CFRP plate and the peeling strength of the adhesive bonding at the notch were investigated by testing several small-scale specimens. The matrix of the test specimens is shown in Table 2.

4.1. Specimens

The dimensions and the material properties of the specimens are same as those in Section 3.1. Only the notch in the middle of the steel beams was considered in the experimental study. To prevent premature flange buckling and web crushing, four 4 mm thick steel stiffeners were welded to each beam at two loading points, one either side of the web. The bonding surfaces of both steel beam and CFRP plate of each retrofitted specimen were first sand blasted to the Sa3 industry standard thoroughly. The CFRP plate was then attached within four hours. The adhesive used was a two-part thixotropic epoxy resin epoxy adhesive (Sikadur-30 Normal). It was mixed with 1% by weight 1 mm diameter ballotini to ensure a uniform bond thickness. Each retrofitted specimen was cured for at least 72 h before testing.

4.2. Test set-up and procedure

The tests were carried out in a servo-hydraulic SDS500 test machine with a maximum capacity of 500 kN, subjected to a four-point bending set up. The specimens were tested under static load, by displacement control at a rate of 0.05 mm/s. Loading of the specimen continued even after the CFRP plate peeling, which occurred in all retrofitted specimens. Loading was stopped when local post-yield buckling appeared in the control specimen or when the notched specimens fractured with the notch propagation.

For the retrofitted beams, the strain distribution in the bottom of the CFRP plate was measured using nine 2 mm long strain gauges mounted along the longitudinal centre line of the CFRP plate (G1–G9 shown in Fig. 8), and five 2 mm long strain gauges were mounted on the steel beam – four on the flanges and one on the web in the middle of the specimens (G10–G14 shown in Fig. 8). For the notched steel beams A-1 and A-2, one strain gauge G10 was mounted at the notch tip. Deflections were measured at middle of the specimens using a potentiometer as shown in Fig. 9. Two loading sensors were installed at the loading points, as shown in Fig. 9. All data were automatically recorded by a data logging system (TDS-530). A camera was used to monitor the debonding progress in the adhesive layer from the notch location. During loading, the strains, displacements, load and the photos were recorded every 1 s.

5. Test results and discussion

Six specimens, including one control beam(C-1), two notched beam(A-1, A-2) and three notched beam strengthened with CFRP plate(AR-1, AR-2, AR-3), were tested. A summary of the test results including the ultimate strengths with their associated deflections, and the failure modes are given in Table 2. The debonding strength and the corresponding maximum interfacial stresses at the notch location calculated in accordance with Section 2 were included in Table 3.

5.1. Strength and stiffness of the specimens

The load versus displacement plots of the specimens are shown in Fig. 10. Two aspects are noted from Fig. 10. Firstly, the stiffness and strength of the notched beams A-1and A-2 is far less than the control beam C-1. Moreover, the retrofitted beams AR-1, AR-2 and AR-3 showed a significant strength and stiffness enhancement over the notched beams, and the stiffness closed to the control beam

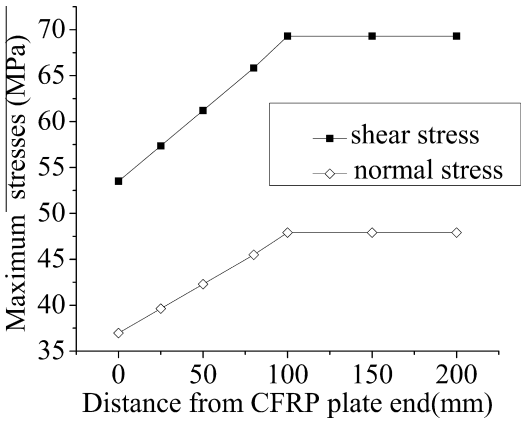

Fig. 6. Maximum interfacial stresses with different notch locations.

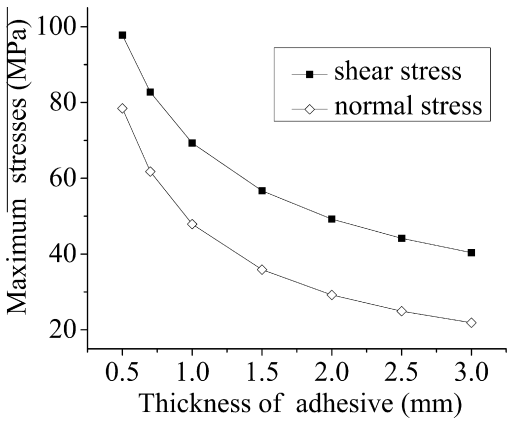

Fig. 7. Maximum interfacial stresses with different thicknesses.

Table 2
Specimen details and test results.

Specimen	Notch	Repair	Ultimate load (kN)	Deflection (mm)	Failure mode
C-1	Without	No	52.9	37.2	Steel buckling
A-1	With	No	21.5	4.6	Notch propagation
A-2	With	No	22.2	5.3	Notch propagation
AR-1	With	Yes	41.0	6.1	CFRP debonding
AR-2	With	Yes	40.9	5.2	CFRP debonding
AR-3	With	Yes	40.4	5.5	CFRP debonding

during elastic stage. Secondly, all the retrofitted beams failed by plate debonding, and after attaining a peak the load dropped suddenly and the load–displacement plot then after followed closely the response of the notched beams. This shows that the CFRP plate strengthening can effectively restore the flexural capacity of notched beams before the plate peeling from the beams.

The maximum loads and their corresponding deflections are given in Table 2. It can be observed that: the average maximum loads of the notched beams and the retrofitted beams are 21.9 kN and 40.8 kN, respectively, which are 41.3% and 77.1% of the maximum loads of the control beam; the average deflections under the maximum loads of the notched beams and the retrofitted beams are 5.0 mm and 5.6 mm, respectively, which are close but far less than that of the control beam. It indicates the strength of the notched beam can be improved almost twice by the CFRP plate strengthening, while the brittle fracture caused by debonding limits the ductility enhancement of the retrofitted beams.

5.2. Strains of the specimens

The strains at the notch tip recorded in gauge G10 of the notched beams and the retrofitted beams are compared in Fig. 11. This figure shows that the strains at the notch tip of the notched beams increased with the loads significantly rapider than those of the retrofitted beams, which indicates that the CFRP plate strengthening restricts the notch opening and hence improves the stiffness of the notched sections.

The CFRP plate in the retrofitted beams peeled from the beams at the maximum loads (see Table 2 and Fig. 10). The strains in all stain gauges on the plate dropped to zero within a very short time, indicating that the peeling was instantaneous. The strains in the plate recorded are shown in Figs. 12–14, from which the following observation can be made:

- The specimens had a linear behaviour up to the yielding of notch tip in the steel beams at approximately 15 kN in accordance with the strain recorded in G10.
- The strains in G5 at mid-span increase almost linearly with the loads. With the load increasing, especially after the steel beam yield, however, plasticity of the adhesive near the notch location occurred and the strains increased rapidly in strain gauges G4 and G6. As load continued to increase, debonding propagated from the middle to the sides and the strains in G3 and G7 and then in G2 and G8 started to quickly increase.
- The strains in gauges G1 and G9, close to the ends of CFRP plate, marginally decreased when the loads were greater than about 30 kN. But the strains did not drop to zero, which is the signal of plate debonding at the ends [14].

Therefore, the strains on the plate in the pure bending section of the beams increased gradually until close to the strain in the middle of the plate.

The longitudinal strain distributions in the CFRP plate at different load levels are shown in Figs. 15–17. When the loads were lower than the debonding loads, the strain concentration at the notch location in the middle of the beam can be observed in the figures. After the loads were higher than the debonding loads, the maximum strain zone spread toward from the middle of the plate to the sides, which indicates the plastication of the adhesive and then the onset of debonding from the notch location as well as what indicated in Figs. 12–14.

The strains measured in gauges G5 and G11–14, in the middle of specimen AR-2, at different load levels are compared in Fig. 18. Since the stress concentration and premature plasication at the notch tip, G10 is not considered in the figures. It can be seen that the strain in the middle section of the specimen is keep linear until the debonding loads applied. This means that prior to debonding initiation, the plane section assumption is adaptive. Similar results were obtained from the other retrofitted specimens AR-1 and AR-3.

5.3. Failure modes of the specimens

The control beam was failed due to beam flange buckling. The notched beams A-1 and A-2 were fractured after the notch in the middle spans propagated to the upper flange. The failure modes of the strengthened notched beams were the CFRP plate peeling but part of it remained attached to the beam. The typical failed specimen AR-3 was showed in Fig. 19.

A camera was used to record the progress of the failure of the strengthened beams. The records show the debonding initiated in the adhesive at the notch location when the loads increased to 32.5 kN, 34.4 kN and 38.7 kN, respectively, which are defined as debonding loads. With the load increasing, the debonding propagated along the interface between the adhesive and CFRP plate toward to the ends of the plate. When the debonding developed close to the loading points, the debonding quickly propagated

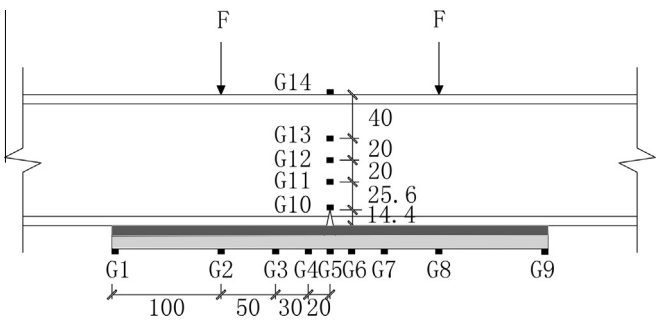

Fig. 8. Strain gauges arrangement for Specimens.

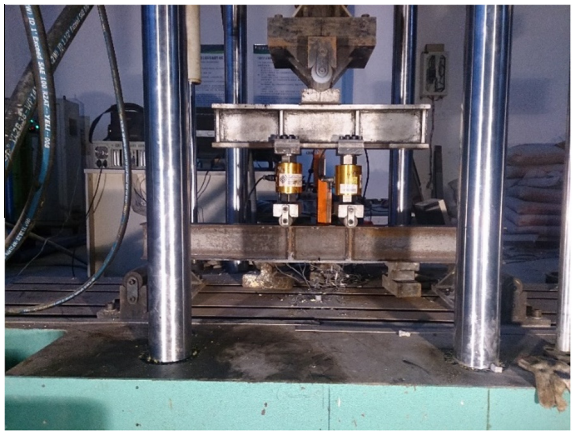

Fig. 9. Test setup.

Table 3
Results of the maximum interfacial stresses.

Specimen	Debonding load (kN)	Maximum shear stress (MPa)	Maximum normal stress (MPa)	Maximum tensile principle stress (MPa)
AR-1	32.5	63.1	43.3	45.1
AR-2	34.4	65.2	44.1	46.8
AR-3	38.7	74.1	50.5	53.0

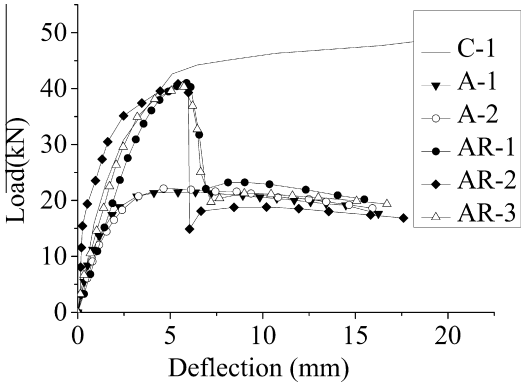

Fig. 10. Load–deflection curves.

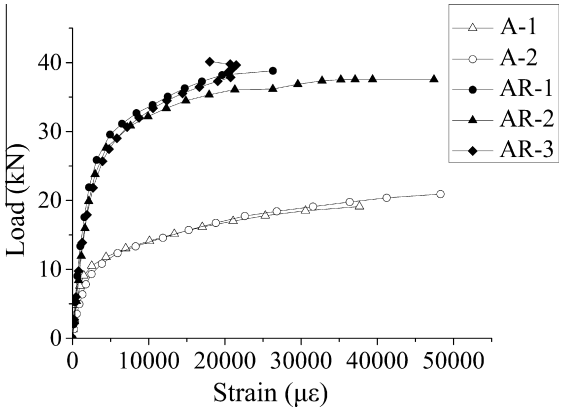

Fig. 11. Load–strain curves.

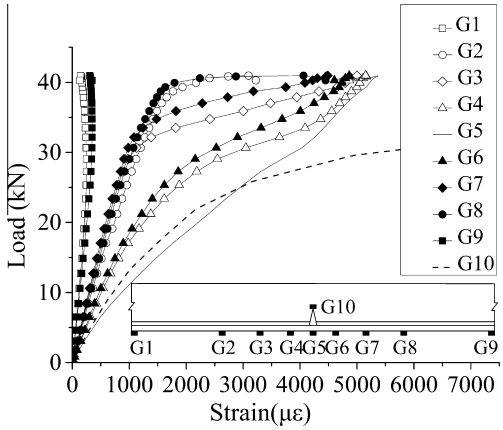

Fig. 12. Strain in the CFRP plate in specimen AR-1.

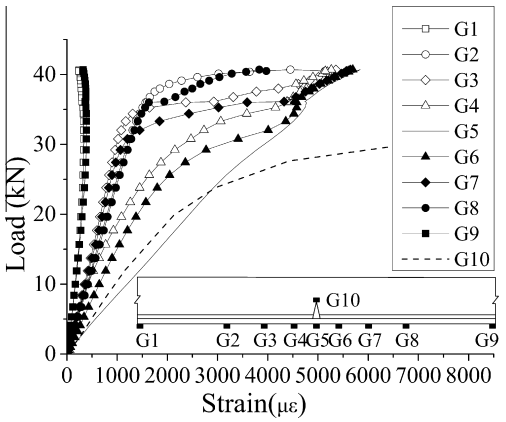

Fig. 13. Strain in the CFRP plate in specimen AR-2.

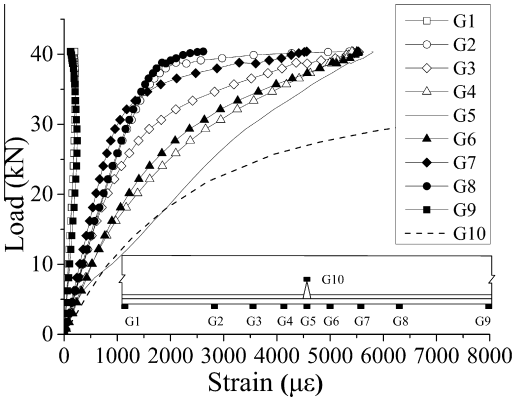

Fig. 14. Strain in the CFRP plate in specimen AR-3.

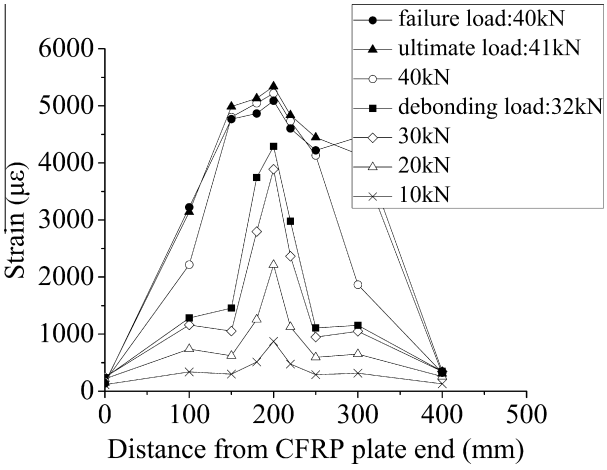

Fig. 15. Strain distributions in CFRP plate at different load levels.

following by one end of the pate rapid peeled and the part of other end remained attached. The strain on the plate measured during the test dropped to zero instantaneously. The load–deflection plots in Fig. 10 indicate that the load suddenly dropped when the CFRP plates were peeling from the steel beams. The notch in the middle of the steel beams did not propagate until the CFRP plate peeled from the steel beam.

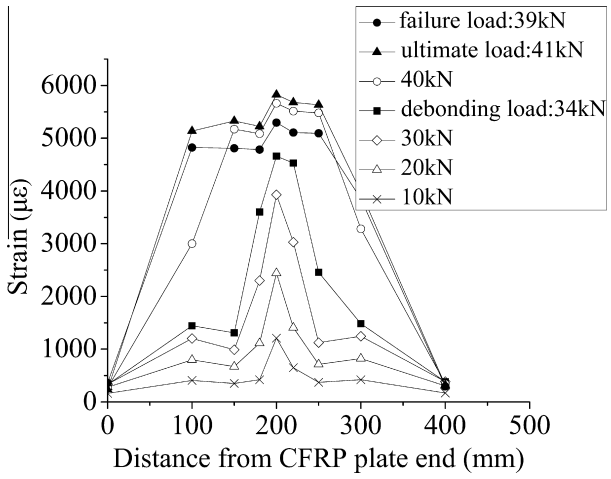

Fig. 16. Strain distributions in CFRP plate at different load levels.

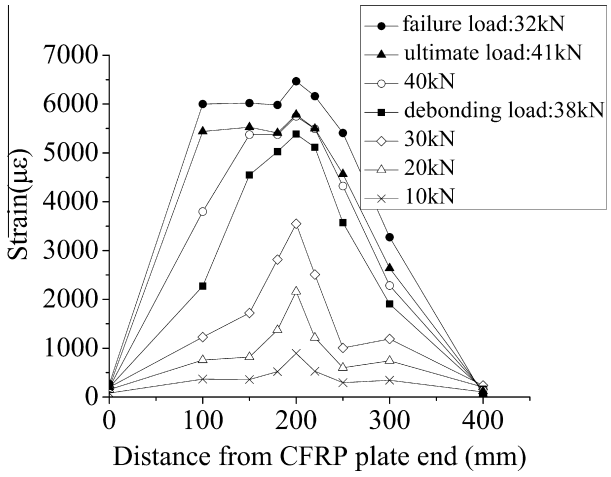

Fig. 17. Strain distributions in CFRP plate at different load levels.

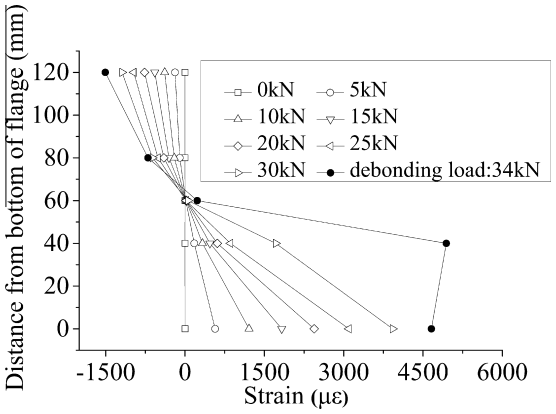

Fig. 18. Strain in the middle of specimen AR-2 at different load levels.

Fig. 19. Typical failure mode (specimenAR-3).

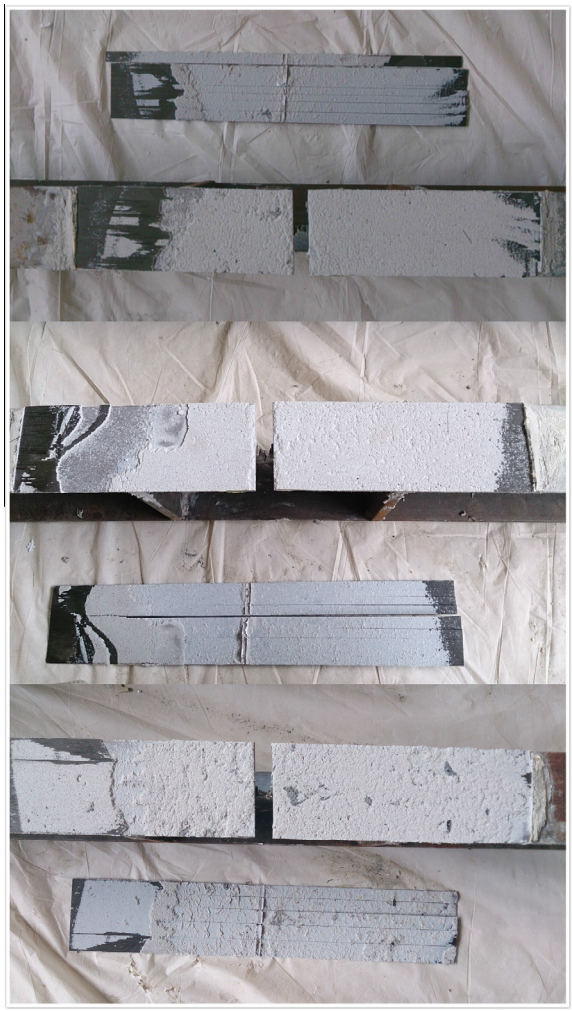

Fig. 20. The debonded specimens AR-1, AR-2 and AR-3.

Fig. 20 shows the bonded surfaces of the CFRP plate and steel beams of the failed specimens which the CFRP plates were detached totally from the steel beam by hand. The figure shows that debonding developed from the notch in the steel beams along the interface between the CFRP plate and the adhesive, but mixture failure (combination of adhesive failure on both interfaces, cohesive failure and delaminate failure in CFRP plate) irregularly occurred when debonding progressed to the left end where remained attached on the steel beam. Deng and Lee [16] show the stress concentration at the plate end in CFRP plate strengthened steel beam causes the debonding progressing along the interface between steel beam and adhesive. In this paper, the stress

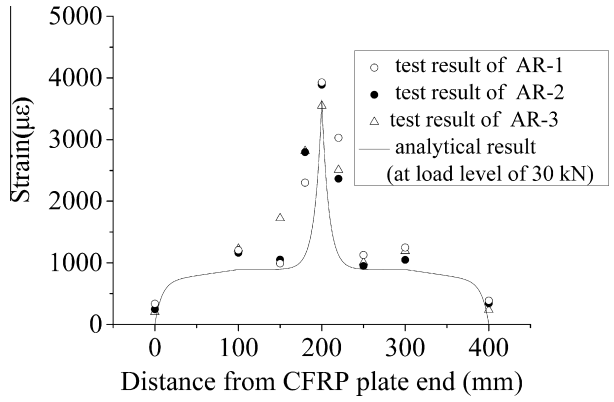

Fig. 21. Comparisons of experimental and analytical strains at load level of 30 kN.

concentration at the interface between CFRP plate and adhesive near the notch, which causes debonding occurred in different interface.

5.4. Validating analytical analysis

The longitudinal strain distributions in the CFRP plate obtained from the tests are compared to the corresponding analytical result, calculated from the theory detailed in Section 2 at the load level of 30 kN, in Fig. 21. The figure shows that the agreement is good.

The maximum principle interfacial stress occurring at the notch in the middle of the specimens causes the debonding initiation. These maximum stresses for all strengthened specimens under the debonding loads in the tests are calculated analytically in accordance with Section 2. The measured thickness of the adhesive in the specimens AR-1, AR-2 and AR-3 are 1.02 mm, 1.10 mm and 1.06 mm, respectively. The analytical results are shown in Table 3. The average value is 94.1 MPa.

6. Conclusions

In this paper, an integrated closed-form solution to calculate the interfacial stresses of steel beams strengthened with CFRP plates has been presented and the expressions of the maximum interfacial stresses at the notch locations, the adhesive hollows and the plate ends are given. Analytical results showed that the interfacial stress concentrations at the notch location is about four times than those at the ends of the plate, which indicates that the stress concentration at notch locations is the major weakness of the strengthened deficient steel beams. The parametric study indicates that the maximum stresses at the notch locations increased with the notch depth and the applied bending moment on notched cross-sections, but reduced with the thickness of the adhesive.

An experimental study has been reported as well. One control beam, two notched beam and three notched beam strengthened with CFRP plate, were tested. The test results show the strength of the notched beam can be improved almost twice by the CFRP plate strengthening, while the brittle fracture caused by debonding limits the ductility enhancement of the retrofitted beams. The strain distribution on the plate indicates that he CFRP plate strengthening restricts the notch opening. After the loads were higher than the debonding loads, the maximum strain zone spread toward from the middle of the plate to the sides and then the onset of debonding along the interface between the adhesive and CFRP plate from the middle notch of the steel beam. The failure modes of the strengthened notched beams were the CFRP plate peeling but part of it remained attached to the beam.

The good agreement between the longitudinal strain distributions in the CFRP plate obtained from the tests and the corresponding analytical results demonstrates the validity of the theory.

Acknowledgements

This work is supported by the National Natural Science Foundation of China through grants 51278131, Program for New Century Excellent Talents in University through grant NCET-13-0739 and Fok Ying Tong Education Foundation through grant 131073.

References

[1] Hollaway LC, Cadei J. Progress in the technique of upgrading metallic structures with advanced polymer composites. Prog Struct Mat Eng 2002;4(2):131–48.
[2] Deng J, Lee MMK. Adhesive bonding in steel beams strengthened with CFRP. Proc Inst Civ Eng Struct Build 2009;162(4):241–9.
[3] Kim YJ, Brunell G. Interaction between CFRP-repair and initial damage of wide-flange steel beams subjected to three-point bending. Compos Struct 2011;93(8):1986–96.
[4] Zhao XL, Zhang L. State of the art review on FRP strengthened steel structures. Eng Struct 2007;29(8):1808–23.
[5] Teng JG, Yu T, Fernando D. Strengthening of steel structures with fiber-reinforced polymer composites. J Constr Steel Res 2012;78:131–43.
[6] Rizkalla S, Dawood M, Schnerch D. Development of a carbon-fiber-reinforced polymer system for strengthening steel structures. Compos A 2008;39(2):388–97.
[7] Colombi P, Poggi C. An experimental, analytical and numerical study of the static behavior of steel beams reinforced by pultruded CFRP strips. Compos B 2006;37(1):64–73.
[8] Sen R, Liby L, Mullins G. Strengthening steel bridge sections using CFRP laminates. Compos B 2001;32(4):309–22.
[9] Deng J, Lee MMK, Li S. Flexural strength of steel–concrete composite beams reinforced with a prestressed CFRP plate. Constr Build Mater 2011;25(1):379–84.
[10] Shaat A, Fam A. Repair of cracked steel girders connected to concrete slabs using carbon-fiber-reinforced polymer sheets. J Compos Constr 2008;12(6):650–9.
[11] Hmidan A, Kim YJ, Yazdani S. CFRP repair of steel beams with various initial crack configurations. J Compos Constr 2011;15(6):952–62.
[12] Buyukozturk O, Gunes O, Karaca E. Progress on understanding debonding problems in reinforced concrete and steel members strengthened using FRP composites. Constr Build Mater 2004;18(1):9–19.
[13] Smith ST, Teng JG. Interfacial stresses in plated beams. Eng Struct 2001;23:857–71.
[14] Deng J, Lee MMK. Behaviour under static loading of metallic beams reinforced with a bonded CFRP plate. Compos Struct 2007;78(2):232–42.
[15] Deng J, Lee MMK, Moy S. Stress analysis of steel beams reinforced with a bonded CFRP plate. Compos Struct 2004;65(2):205–15.
[16] Deng J, Lee MMK. Effect of plate end and adhesive spew geometries on stresses in retrofitted beams bonded with a CFRP plate. Compos B Eng 2008;39(4):731–9.
[17] Teng JG, Fernando D, Yu T. Finite element modelling of debonding failures in steel beams flexurally strengthened with CFRP laminates. Eng Struct 2015;86:213–24.
[18] Kim YJ, Harries KA. Predictive response of notched steel beams repaired with CFRP strips including bond-slip behaviour. Int J Struct Stab Dyn 2012;12(1):1–21.
[19] Zhou H, Attard TL, Wang Y, Wang JA, Ren F. Rehabilitation of notch damaged steel beams using a carbon fiber reinforced hybrid polymeric-matrix composite. Compos Struct 2013;106:690–702.
[20] Deng J, Lee MMK. Fatigue performance of metallic beams strengthened with bonded CFRP plates. Compos Struct 2007;78(2):222–31.
[21] Colombi P, Fava G. Experimental study on the fatigue behaviour of cracked steel beams repaired with CFRP plates. Eng Fract Mech 2015;145:128–42.